INTERNATIONAL JOURNAL OF CLIMATOLOGY
Int. J. Climatol. (2017)
Published online in Wiley Online Library
(wileyonlinelibrary.com) DOI: 10.1002/joc.5334

RMetS
Royal Meteorological Society

Evaluation and projection of extreme precipitation indices in the Eastern Mediterranean based on CMIP5 multi-model ensemble

Rana Samuels,[a,‡,§] Assaf Hochman,[a,b,c*,†] Anat Baharad,[d,†] Amir Givati,[e] Yoav Levi,[d] Yizhak Yosef,[a,d] Hadas Saaroni,[c] Baruch Ziv,[a] Tzvika Harpaz[a,c] and Pinhas Alpert[a]

[a] *Department of Geophysics, School of Geosciences, Tel-Aviv University, Israel*
[b] *Porter School of Environmental Studies, School of Geosciences, Tel-Aviv University, Israel*
[c] *Department of Geography and the Human Environment, School of Geosciences, Tel-Aviv University, Israel*
[d] *Israel Meteorological Service, Beit Dagan, Israel*
[e] *Israel Hydrological Service, Israel Water Authority, Jerusalem, Israel*

ABSTRACT: An evaluation of 23 models, participating in the Coupled Model Inter-comparison Project phase 5 (CMIP5), in representing extreme precipitation indices (EPI), over the Eastern Mediterranean (EM) and the Fertile Crescent (FC), was performed. The models ensemble was then used to predict the EPIs evolution in the 21st century under (Representative Concentration Pathway, RCP) RCP4.5 and RCP8.5 scenarios. Models' performance was determined with respect to gridded precipitation observations from the APHRODITE project. The ensemble mean was found to perform relatively well in capturing the EM steep precipitation gradient, the FC structure and the EPI trends in the observations period (1970–2000). Over the EM, CMIP5 models agree on a future decrease in the following three EPIs; total precipitation (TP), consecutive wet days, and number of wet days by the values of 20–35%, 10–20%, and 20–35%, respectively. In the FC, extremely wet days (P95) are expected to increase by approximately 25%, except for the south eastern coasts of the Mediterranean Sea, which show significant decreases in P95, particularly for RCP8.5 and at the end of the 21st century. Hence, while TP is expected to decrease, extreme precipitation is expected to increase, at least for the north-eastern part of the FC. This will significantly influence agriculture and floods' potential in a region already suffering from political unrest. The changes in EPIs are related to changes in the synoptic patterns over the EM, especially the predicted changes in cyclones frequency and intensity in the 21st century, due to changes in storm tracks governed by the phase of the North Atlantic Oscillation and the expected expansion of the Hadley Cell towards the poles in a warmer climate.

KEY WORDS CMIP5; model ensemble; climate models; Eastern Mediterranean; extreme precipitation indices; Fertile Crescent

Received 15 January 2017; Revised 30 August 2017; Accepted 3 October 2017

1. Introduction

Simulations from state-of-the-art global climate models (GCM) (Table 1) are available for analysis within the Coupled Model Inter-comparison Project Phase 5 (CMIP5) (Taylor *et al.,* 2012), which includes models with a higher spatial resolution than CMIP3 (Meehl *et al.,* 2007), allowing the scientific community to address a wider variety of research questions focusing on climate changes (Sillman *et al.,* 2013a, 2013b). Given the differences in the models' structure and physical equations, it is expected that models would perform differently over different regions of the world. One important task is to not only evaluate CMIP5 for the different aspects of mean climate, but also for extreme climate and weather events (Sillman *et al.,* 2013a).

While extreme weather events have many aspects, this study's focus is on precipitation extremes indices, with the emphasis given to the daily time-scale. Extreme precipitation events, and their potential changes have an essential influence on human life, economy, and ecosystems, especially in the Eastern Mediterranean (EM) (Ziv *et al.,* 2014; Kelley *et al.,* 2015). While monthly means provide useful information on gross climate changes, the environmental impact is often the result of short-term phenomena occurring well into the distribution tails of daily data (Zhang *et al.,* 2011). In order to gain a uniform perspective on observed changes in weather and climate extremes, an internationally coordinated core set of 27 indices for moderate temperature and precipitation extremes was defined by the Expert Team on Climate Change Detection and Indices (ETCCDI; Klein Tank *et al.,* 2009, Zhang *et al.,* 2011). These extreme indices find multiple applications in climate research due to their statistically robustness

* Correspondence to: A. Hochman, Department of Geophysics, School of Geosciences, Tel-Aviv University, Tel Aviv 69978, Israel.
E-mail: assafhochman@post.tau.ac.il; assafhochman@yahoo.com

† These authors contributed equally.
‡ This article is dedicated to Rana Samuels blessed memory.
§ Deceased.

Table 1. The 23 CMIP5 models in the present study with the following listing columns; modelling center (or group), institute ID, model name, and horizontal resolution (°) following Taylor *et al.* (2012).

Modelling center (or group)	Institute ID	Model name	Resolution (°)
Commonwealth Scientific and Industrial Research Organization (CSIRO) and Bureau of Meteorology (BOM), Australia	CSIRO-BOM	ACCESS1.0	1.25 × 1.875
Beijing Climate Center, China Meteorological Administration	BCC	BCC-CSM1.1	2.7906 × 2.8125
College of Global Change and Earth System Science, Beijing Normal University	GCESS	BNU-ESM	2.7906 × 2.8125
Canadian Centre for Climate Modelling and Analysis	CCCMA	CanESM2	2.7906 × 2.8125
National Center for Atmospheric Research	NCAR	CCSM4	0.9424 × 1.25
Community Earth System Model Contributors	NSF-DOE-NCAR	CESM1(BGC)	0.9424 × 1.25
Centro Euro-Mediterraneo per I Cambiamenti Climatici	CMCC	CMCC-CMS	3.711 × 3.75
Centre National de Recherches Météorologiques/Centre Européen de Recherche et Formation Avancée en Calcul Scientifique	CNRM-CERFACS	CNRM-CM5	1.4008 × 1.40625
NOAA Geophysical Fluid Dynamics Laboratory	NOAA GFDL	GFDL-ESM2G	2.0225 × 2
		GFDL-ESM2M	2.0225 × 2.5
		GFDL-CM3	2 × 2.5
Met Office Hadley Centre (additional HadGEM2-ES realizations contributed by Instituto Nacional de Pesquisas Espaciais)	MOHC (additional realizations by INPE)	HadCM3	3.75 × 2.5
		HadGEM2-CC	1.25 × 1.875
		HadGEM2-ES	1.25 × 1.875
Institute for Numerical Mathematics, Spain	INM	INM-CM4	1.5 × 2
Institut Pierre-Simon Laplace, France	IPSL	IPSL-CM5A-LR	1.8947 × 3.75
		IPSL-CM5B-LR	1.8947 × 3.75
Japan Agency for Marine-Earth Science and Technology, Atmosphere and Ocean Research Institute (The University of Tokyo), and National Institute for Environmental Studies	MIROC	MIROC-ESM	2.7906 × 2.8125
Atmosphere and Ocean Research Institute (The University of Tokyo), National Institute for Environmental Studies, and Japan Agency for Marine-Earth Science and Technology	MIROC	MIROC4h	0.5616 × 0.5625
		MIROC5	1.4008 × 1.40625
Max-Planck-Institut für Meteorologie (Max Planck Institute for Meteorology)	MPI-M	MPI-ESM-MR	1.8653 × 1.875
		MPI-ESM-LR	1.8653 × 1.875
Meteorological Research Institute, Japan	MRI	MRI-CGCM3	1.12148 × 1.125

and a wide range of the climate covered. The use of these indices in the literature was reviewed by Zhang *et al.* (2011). Studies have shown that extreme precipitation events are expected to increase in future scenarios (Tebaldi *et al.,* 2006; Sillman and Roeckner, 2008). The indices considered in this study represent a subset of the ETCCDI ones. Twelve Extreme Precipitation Indices (EPI) (Table 2), have been selected from those widely used in the literature (Samuels *et al.,* 2011; Smiatek *et al.,* 2011; Soares *et al.,* 2012; Domínguez *et al.,* 2013; Givati and Rosenfeld, 2013; Turco *et al.,* 2013; Zollo *et al.,* 2016). Seven of the 12 EPIs are calculated in days, therefore provide approximations of dry and wet spell durations. The other five EPIs are calculated in millimetre, therefore offer estimations of heavy and light precipitation events. Some of the indices were modified to fit the annual cycle of precipitation in the EM.

The EM is located on the border between a temperate climate, in its northern part and an arid climate in its south, making it vulnerable to precipitation variations (Giorgi and Lionello, 2008). The EM climate conditions are characterized by moderate air temperatures and rainy spells during the cooler winter season and dry and stable hot weather during the summer. The region's climate is strongly affected by external forcing of both mid latitude and tropical origins (Alpert *et al.,* 2005). Most of the annual precipitation is obtained during a limited number of rain days. The rainy events are typically associated with intrusions of cold air masses from European origin that cross the relatively warm Mediterranean Sea, associated with the Cyprus Lows (Alpert *et al.,* 1990; Saaroni *et al.,* 2010; Ziv *et al.,* 2015). Penetration of warm humid masses originating from tropical Atlantic and/or equatorial regions of Eastern Africa and Arabian Sea contribute as well to rain events, mostly severe ones (Krichak *et al.,* 2004, 2015; Shalev *et al.,* 2011; De Vries *et al.,* 2013). Topography and coastal features (with windward effects, gap winds, land-sea breezes, etc.) also influence the spatial distribution of climate characteristics in the region (Krichak *et al.,* 2010).

Alpert *et al.* (2002) and Zhang *et al.* (2005) calculated EM trends in present daily precipitation indices. They

Table 2. EPI used in this study and their definition following Sillman *et al.* (2013a).

Index number	Label	Name	Definition	Units
1	TP	Total precipitation	Let PR*ij* be the daily precipitation amount on a wet day *i* in period *j*. If *I* represents the number of days in *j*, then: TP = $\sum_{n=1}^{I} PRij$	mm
2	R1mm	Number of wet days	Let PR*ij* be the daily precipitation amount on day *I* in period *j*. Count the number of days were PR*ij* > 1 mm.	days
3	P90	Very wet days	Let PR*wj* be the daily precipitation amount on a wet day *w* (PR ≥ 1 mm) in period *j* and let PR*wn*90 be the 90th percentile of precipitation in wet days in the 1961–1990 period. If W represents the number of wet days in the period, where: PR*wj* > PR*wn*90 then: P90 = $\sum_{w=1}^{W}$ PR*wj*	mm
4	P95	Extremely wet days	Let PR*wj* be the daily precipitation amount on a wet day *w* (PR ≥ 1 mm) in period *j* and let PR*wn*95 be the 95th percentile of precipitation in wet days in the 1961–1990 period. If W represents the number of wet days in the period, where PR*wj* > PR*wn*95 then: P95 = $\sum_{w=1}^{W} PRwj$	mm
5	P10	Driest wet days	Let PR*wj* be the daily precipitation amount on a wet day *w* (PR ≥ 1 mm) in period *j* and let PRwn10 be the tenth percentile of precipitation in wet days in the 1961–1990 period. If W represents the number of wet days in the period, where PR*wj* < PR*wn*10 then: P10 = $\sum_{w=1}^{W} PRwj$	mm
6	P50	Median wet days	Let PR*wj* be the daily precipitation amount on a wet day *w* (PR ≥ 1 mm) in period *j* and let PRwn50 be the 50th percentile of precipitation in wet days in the 1961–1990 period. If W represents the number of wet days in the period, where PR*wj* = PR*wn*50 then: P50 = $\sum_{w=1}^{W} PRwj$	mm
7	CWD	Consecutive wet days	Let PR*ij* be the daily precipitation amount on day *i* in period *j*. Count the largest number of consecutive days where PR*ij* > 1 mm	days
8	CWDmx	Maximum number of consecutive wet days	Let PR*ij* be the daily precipitation amount on day *i* in period *j*. CWDmx is the maximum number of consecutive wet days for the period 1970–2000, where PR*ij* > 1 mm.	days
9	CWDDJF	Consecutive winter (DJF) wet days	Let PR*ij* be the daily precipitation amount on day *i* in period *j*. Count the largest number of consecutive wet days in the winter (DJF), where PR*ij* > 1 mm	days
10	CWDDJFmx	Maximum number of consecutive winter (DJF) wet days	Let PR*ij* be the daily precipitation amount on day *i* in period *j*. CWDDJFmx is the maximum number of consecutive wet days in the winter (DJF) for the period 1970–2000, where PR*ij* > 1 mm.	days
11	CDDDJF	Consecutive winter (DJF) dry days	Let PR*ij* be the daily precipitation amount on day *i* in period *j*. Count the largest number of consecutive days in the winter (DJF) where PR*ij* < 1 mm	days
12	CDDDJFmx	Maximum number of consecutive winter (DJF) dry days	Let PR*ij* be the daily precipitation amount on day *i* in period *j*. CDDDJFmx is the maximum number of consecutive dry days in the winter (DJF) for the period 1970–2000, where PR*ij* < 1 mm.	days

found weak trends in general, and without spatial coherence. Alpert *et al.* (2008) analysed regional climate models for the EM and predicted large significant precipitation decreases over the Mediterranean and Northern Israel. Kitoh *et al.* (2008), employing a high resolution (20 km) GCM, predicted that the Fertile Crescent (FC), also known as the cradle of civilization, which is a crescent-shaped fertile land region containing the comparatively moist area of otherwise arid and semi-arid western Asia as well as the Nile Valley and its Delta (marked in black in Figure 1), will probably change its shape or disappear altogether by the end of the 21st century. Chenoweth *et al.* (2011) showed that a decrease of about 10% in mean annual precipitation is expected in the EM by the end of the 21st century, as simulated by the PRECIS model. Lelieveld *et al.* (2012) showed that the annual precipitation is expected to

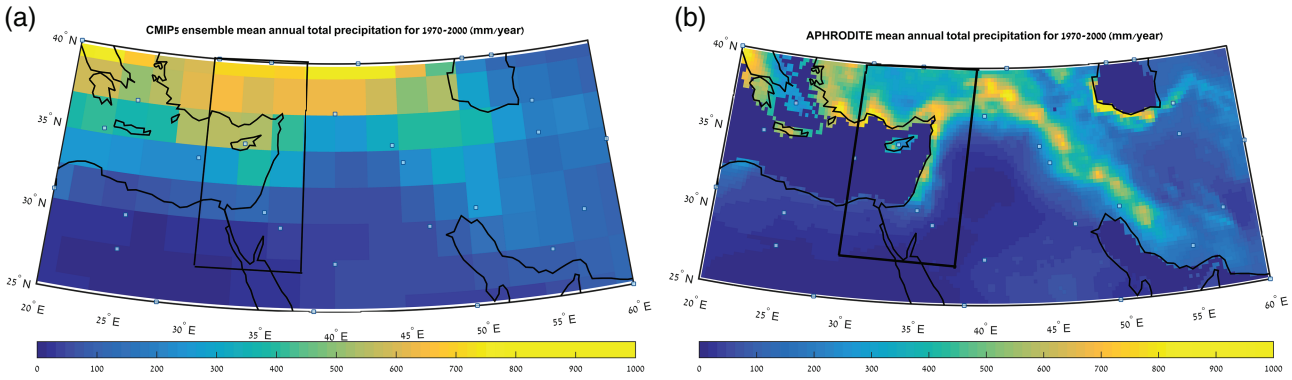

Figure 1. Annual average precipitation (mm/years) maps for the CMIP5 model ensemble mean (a) and for the APHRODITE data set (b). Maps are 30-year averages (1970–2000) for the large area. The small area is marked with a black rectangle.

decrease in Southern Turkey and the Levant, as simulated by PRECIS. Ziv *et al.* (2014) studied the observed trends in precipitation over Israel for the period 1975–2010, and found decreases over the vast majority of Israel, significant only in the super-arid part. Kelley *et al.* (2015) linked the Syrian uprising before 2011 with the unusual long drought in the greater FC. No comprehensive attempt has been made yet to predict future precipitation extremes with an ensemble of CMIP5 models for the EM region.

This study provides an overview of performance and future EPI projections of 23 CMIP5 GCMs for the Middle East with an emphasis on Israel and the FC. The ability of the models in accurately depicting EPIs is dependent on the geographical region chosen for the evaluations and projections of EPIs. For instance, the small and large areas in this study are located on the border of three subregions (Mediterranean, Sahara, and Central Asia) studied in Sillman *et al.* (2013a, 2013b) and in other studies. These subregions have very different climate regimes and are expected to respond differently to global warming (Sillman *et al.,* 2013a, 2013b). This is why a more localized evaluation and projections of the CMIP5 models is provided here.

This paper is organized as follows: Section 2 specifies the observations and modelled data used in this study, Section 3 gives an overview of the methodology, Section 4 presents models evaluation with respect to observations and future predictions for chosen EPI and Section 5 provides a short summary and the main conclusions.

2. Data

Model performance was assessed through comparison with observed high resolution indices calculated from daily precipitation data over the Middle East, created in the framework of the Asian Precipitation Highly Resolved Observational Data Integration Towards Evaluation (APHRODITE) of water resources project (Yatagai *et al.,* 2008, 2012), available in the APHRODITE website (http://www.chikyu.ac.jp/precip). This gridded data set, in a $0.25^\circ \times 0.25^\circ$ resolution, is based on a dense network of rain gages in the Middle East. It was shown that this data can serve as a good evaluating tool for climate models performance (Yatagai *et al.,* 2008, 2012). In addition, when APHRODITE, is compared to other gridded data sets (New *et al.,* 1999; Huffman *et al.,* 2001) it can demonstrate the effect of orography on precipitation (Yatagai *et al.,* 2008, 2012). Uncertainties in APHRODITE data are related to relatively sparse rain gages in the desert and absolutely no information over the seas. Furthermore, APHRODITE does not assimilate information from different sources, but rather from rain gages alone. For instance, it was found that APHRODITE overestimates the wet days and underestimates the dry days over India (Chaudhary *et al.,* 2017) and underestimates the EPI over China with respect to other data sets investigated (Yin *et al.,* 2015).

Modelled daily precipitation data were obtained from the Earth System Grid data portal for 23 CMIP5 models (for list of models see Table 1). Note that single simulations were used from all models, i.e. 'r1i1p1' while the letters 'r,l,p' are standing for r-realization of control run, i-initialization method, and p-perturbed physics. The main improvements in CMIP5 include the addition of interactive ocean and land carbon cycles, more comprehensive modelling of the indirect effect of aerosols and the use of volcanic and solar forcing in most models (Taylor *et al.,* 2012). Models' spatial resolutions range between $0.56^\circ \times 0.56^\circ$ and $3.71^\circ \times 3.75^\circ$.

The analysis is based on the historical simulations of the CMIP5 models for 1970–2000 and present-to-future simulations for 2006–2036 [based on the Representative Concentration Pathway 4.5 (RCP4.5) scenario]. These predictions were initialized based on observations and are used to explore climatic predictability and to assess the forecast system's predictive skill. The other future periods simulated, and analysed, are 2046–2065 and 2081–2100 based on both RCP4.5 and RCP8.5 with respect to the 1986–2005 reference period (IPCC, 2013). The RCPs adopted by the IPCC for its fifth assessment report (AR5) are: RCP2.6, RCP4.5, RCP6, and RCP8.5. They are named after the possible radiative forcing (in $\mathrm{W\,m^{-2}}$) expected in the year 2100 relative to pre-industrial values. RCP2.6 assumes the global greenhouse gas (GHG) emissions will peak between 2010 and 2020 and then will decline, RCP4.5 assumes GHG will peak around 2040,

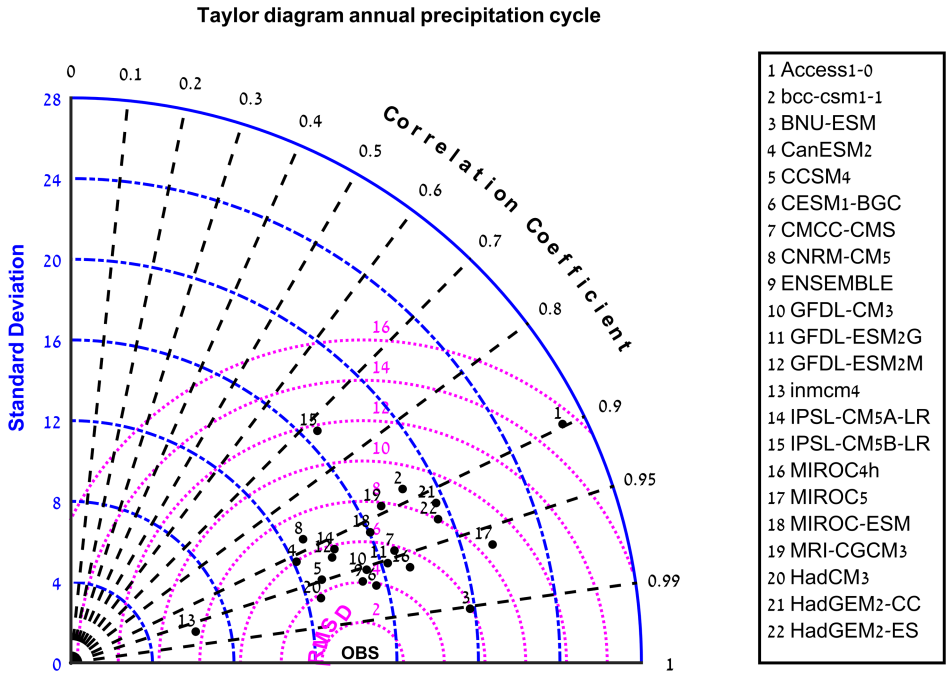

Figure 2. Taylor diagram (Taylor, 2001) comparing between the annual cycle of precipitation for the CMIP5 models and APHRODITE observations in the 1970–2000 period over the small region (see rectangle in Figure 1). The black circles denote the performance of the 22 CMIP5 models with respect to the root mean square difference, standard deviation, and correlation coefficient. [Colour figure can be viewed at wileyonlinelibrary.com].

RCP6 assumes GHG will peak around 2080 and RCP8.5 assumes that GHG will continue to rise throughout the 21st century.

3. Method

Two regions were defined in this study. The 'large study area' ('large' in brevity, see Figure 1) is defined as (25°–40°N; 20°–60°E) and includes the FC, which is a region suffering from political unrest mostly related to conflict over water resources (Kelley *et al.,* 2015). The 'small study area' ('small' in brevity, denoted in Figure 1), covering part of the EM and Israel, and is defined as (27.5°–40°N; 30°–38°E), is a transition zone between temperate climate in the north and arid climate in the south.

First, average annual precipitation was calculated for the region, both for CMIP5 models ensemble mean and for the observations in order to investigate how the different data sets capture the unique shape of the FC and the steep precipitation gradients over the EM and Israel (Figure 1). Furthermore, the ability of the different models in capturing the annual precipitation cycle for the small study area, which was the focus of the study, was evaluated using a Taylor diagram (Figure 2, further discussed in Section 4.1; based on Taylor, 2001). A Taylor diagram can provide a concise statistical summary of how well patterns match each other in terms of their correlation, their root-mean-square difference, and the ratio of their variances.

For each of the models, 12 EPIs were calculated, for present and future. Table 2 lists the EPI, their definition and the way they are calculated. These indices can give an overview of both length of dry/wet spells and intensity of precipitation events. To calculate the bias (in %) between the outputs of the CMIP5 models and the APHRODITE reference data set, a sea-land mask was added to the models, since the APHRODITE data set does not include observations over the sea. A subset of 4 of the 12 EPI [i.e., total precipitation (TP), consecutive wet days (CWD), extremely wet days (P95) and number of wet days (R1mm)] were chosen for further evaluation for trends and variability using time series plots and boxplots. Note that all indices are calculated with $\geq$1 mm for wet days. This threshold excludes very light precipitation days and partially accounts for the limited accuracy of rain gages (Zolina *et al.,* 2013). The 1-mm threshold may still imply uncertainties for the estimation of EPI, especially for the number of wet days and consequently the wet spells index (CWD). The 1-mm threshold in this study is a reasonable threshold as will be shown in the next section. The models' data are available in a variety of spatial resolutions (Table 1), therefore they were linearly interpolated to fit the APHRODITE observational grid (of $0.25° \times 0.25°$).

To evaluate future changes in EPI, the differences between present-to-future (2006–2036) and the historical (1970–2000) simulations were calculated and plotted in a portrait diagram. This was done for the RCP4.5 scenario. Furthermore, a spatial–temporal analysis was produced using the CMIP5 ensemble mean for the four EPI, mentioned above. The differences between future and present simulations were calculated for present-to-future (2006–2036 minus 1970–2000),

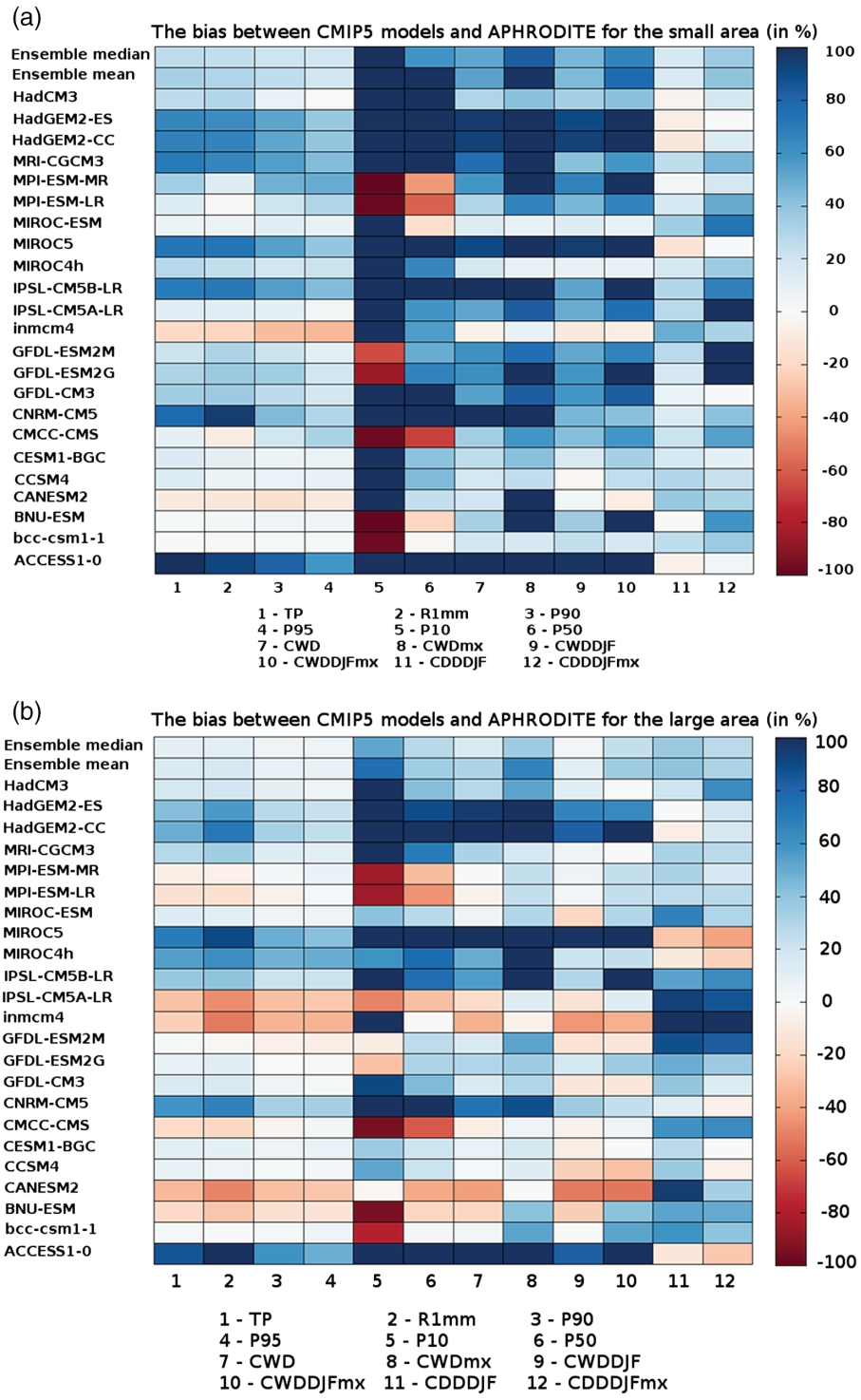

Figure 3. Portrait diagram showing the difference (in %) between the models and APHRODITE data for the 12 EPI for the present period (1970–2000), for the small (a) and large (b) study areas. The list of the 12 EPI is given at the bottom of each figure and are explained in Table 2.

mid-century (2046–2065 minus 1986–2005), and end-century (2081–2100 minus 1986–2005) for the RCP4.5 and RCP8.5 scenarios. Finally, the temporal evolution of the CMIP5 ensemble mean (1861–2100) was calculated for the four declared EPI, for the small study area, as this region is the focus of this study. The trends significance was tested using a simple two tailed *t*-test (at the 95% confidence level).

4. Results

4.1. Evaluation of models' performance against observations

Figure 1 presents average annual precipitation maps (1970–2000) of the models ensemble mean (Figure 1(a)) and of APHRODITE (Figure 1(b)) including the small and large study areas. The APHRODITE data set captures

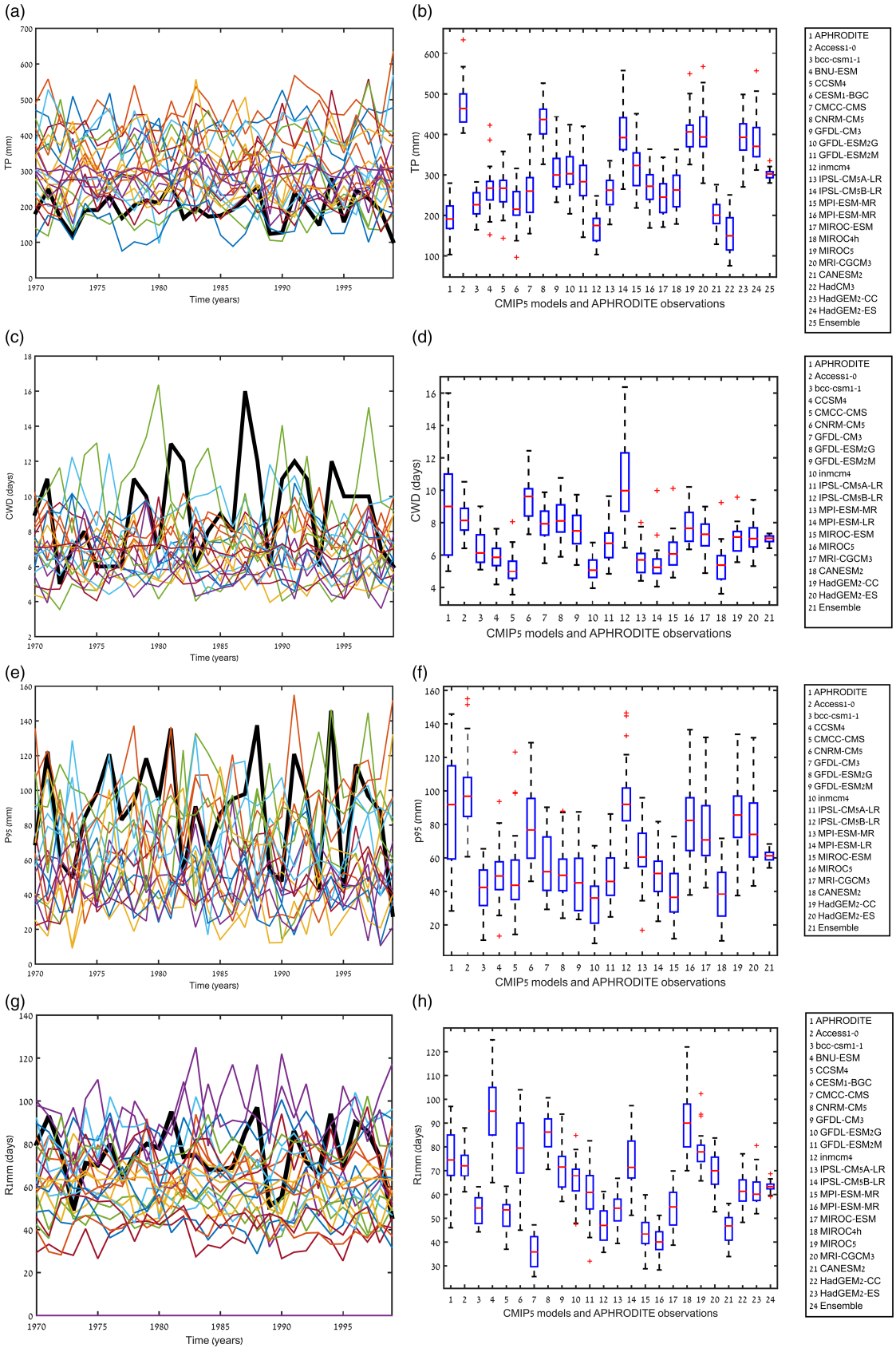

Figure 4. Time series plots (left column) and boxplots (right column) comparing CMIP5 modelled EPI and APHRODITE observed EPIs (1970–2000) for TP (a, b), CWD (c, d), extremely wet days (P95; e, f), and number of wet days (R1mm; g, h). The definition of the EPIs is given in Table 2. APHRODITE observations are indicated with a black bold line. [Colour figure can be viewed at wileyonlinelibrary.com].

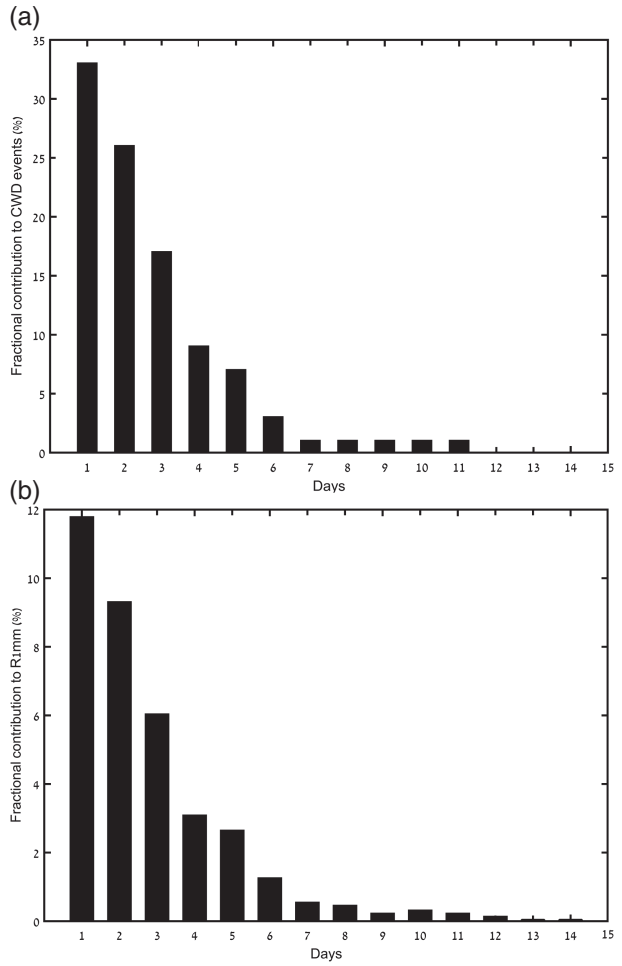

Figure 5. The empirical histograms for the duration of wet spells contribution to the wet spell events (a) and the fractional contribution of the wet spell duration to the total number of wet days (b). The region considered is the small study area shown in Figure 1 derived from APHRODITE data set for 1970–2000.

very well the EM precipitation gradient as well as the shape of the FC (Yatagai *et al.,* 2008). The ensemble mean captures well the shape of the FC, though CMIP5 exhibits an overestimation, presumably due to the limited resolution of the models (∼1–2°), which avoids high-resolution representation of the complex topography for some FC regions, and possibly the exaggerated moisture availability in the cumulus parameterization schemes of the models (Hochman *et al.,* 2017a). The spatial distribution of precipitation as a function of the main orographic features of the EM is better resolved by APHRODITE.

Figure 2 presents a Taylor diagram comparing between the annual cycle of precipitation for the CMIP5 models and APHRODITE observations in the 1970–2000 period over the small study area. Most of the models perform relatively well in capturing the annual cycle of daily precipitation and the ensemble mean of the models is shown to be closest to the APHRODITE observations. ACCESS1-0, IPSL-CM5B-LR and inmcm4 seem to be inferior in this manner.

A portrait diagram is a powerful tool in evaluating individual models with regard to a reference data set (Sillman *et al.,* 2013a, 2013b). Figure 3 presents a portrait diagram for the chosen EPI, which shows the bias in percentage between the models' results and the APHRODITE data set. Blue and red colours represent over and underestimations, respectively. Overestimations of the models when compared with APHRODITE can be easily noticed. There is no single model that performs best for all EPI. Six out of the 23 models (HadGEM2-CC, HadGEM2-ES, MIROC5, IPSL-CM5B-LR, CNRM-CM5 and ACCESS1-0) have considerable overestimations for most of the EPI in both the small (Figure 3(a)) and the large (Figure 3(b)) study areas. This is not surprising for HadGEM2-CC and HadGEM2-ES as they are assumed to share atmospheric and oceanic code. These two models are also located very close to each other on the Taylor diagram, for the same reason (Figure 2). Note that ACCESS1-0 and IPSL-CM5B-LR are shown to be inferior in this manner. For the small study area (Figure 3(a)), only 14 of the 264 rectangle boxes show underestimations, while 39 of the 264 boxes demonstrate underestimations for the large study area (Figure 3(b)). Lower deviations found for the large study area may be explained by widespread desert regions included in that area, which have low density of observations compared to the populated regions included in the small study area. Furthermore, the models seem to perform better in the large study area (Figure 3(b)) than in the smaller one (Figure 3(a)) because in the large one there are larger percentage of regions with no observations, so that the comparison done with the APHRODITE data set is against interpolated precipitation rather than with observations.

Most of the models perform relatively well (bias $< +-20\%$) for total wet days precipitation (TP), number of wet days (R1mm), very wet days (P90), extremely wet days (P95) and consecutive winter dry days (CDDDJF). These results are reflected in the ensemble mean and median percentage biases. Large overestimations are apparent for the driest wet days and for the weak rainy days (P10) in most of the models, except for MPI-ESM-MR, MPI-ESM-LR, GFDL-ESM2M, GFDL-ESM2G, CMCC-CMS, BNU-ESM, and bcc-csm1-1. This is also the case for the Median Wet Days (P50) excluding GFDL-ESM2M and GFDL-ESM2G. The ensemble mean performs poorly, with large overestimations in P10, P50, maximum number of consecutive wet days (CWDmx) and maximum number of consecutive winter wet days (CWDDJFmx). One way to explain the large overestimations (in the order of 100% bias) in the weak rainy days (P10) of the CMIP5 models as compared with APHRODITE observations is the Virga phenomenon, which is the evaporation of rain underneath clouds. Rain gages often miss the weak rains due to Virga, especially in the semi-arid regions, while models with coarser horizontal resolution do not simulate Virga accurately. Therefore producing more rainfall even if the precipitation does not reach the ground (Raich *et al.,* 2017). As expected, the biases are mostly lower for the large study area (Figure 3(b)), typically in the range of −20% to +20%. Moreover, the ensemble mean for the large area performs relatively well

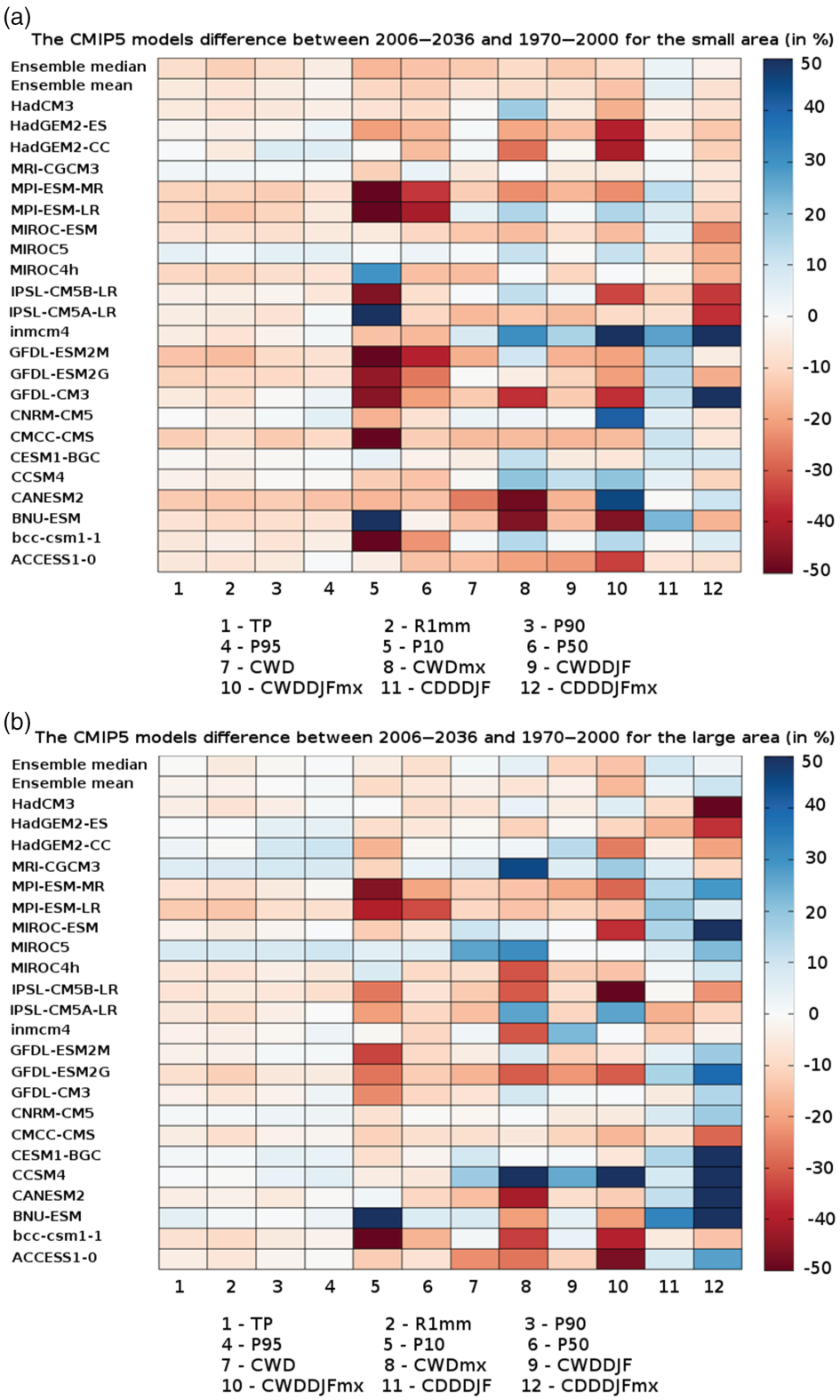

Figure 6. Portrait diagrams showing the difference between present-to-future (2006–2036) (RCP4.5) and past (1970–2000) for various EPIs from the CMIP5 models, for the small (a) and large (b) areas. The definition of the EPIs is given in Table 2.

for most EPI, with bias mostly <20% except for P10 and CWDmx.

Figure 4 displays the models spread in the small study area (1970–2000) in time series plots and boxplots with respect to APHRODITE observations for TP (Figures 4(a) and (b)), CWD (Figures 4(c) and (d)), extremely wet days (P95; Figures 4(e) and (f)) and number of wet days (R1mm; Figures 4(g) and (h)). The trends during the observational period are most similar for the different models shown (Figure 4). Overestimations are apparent

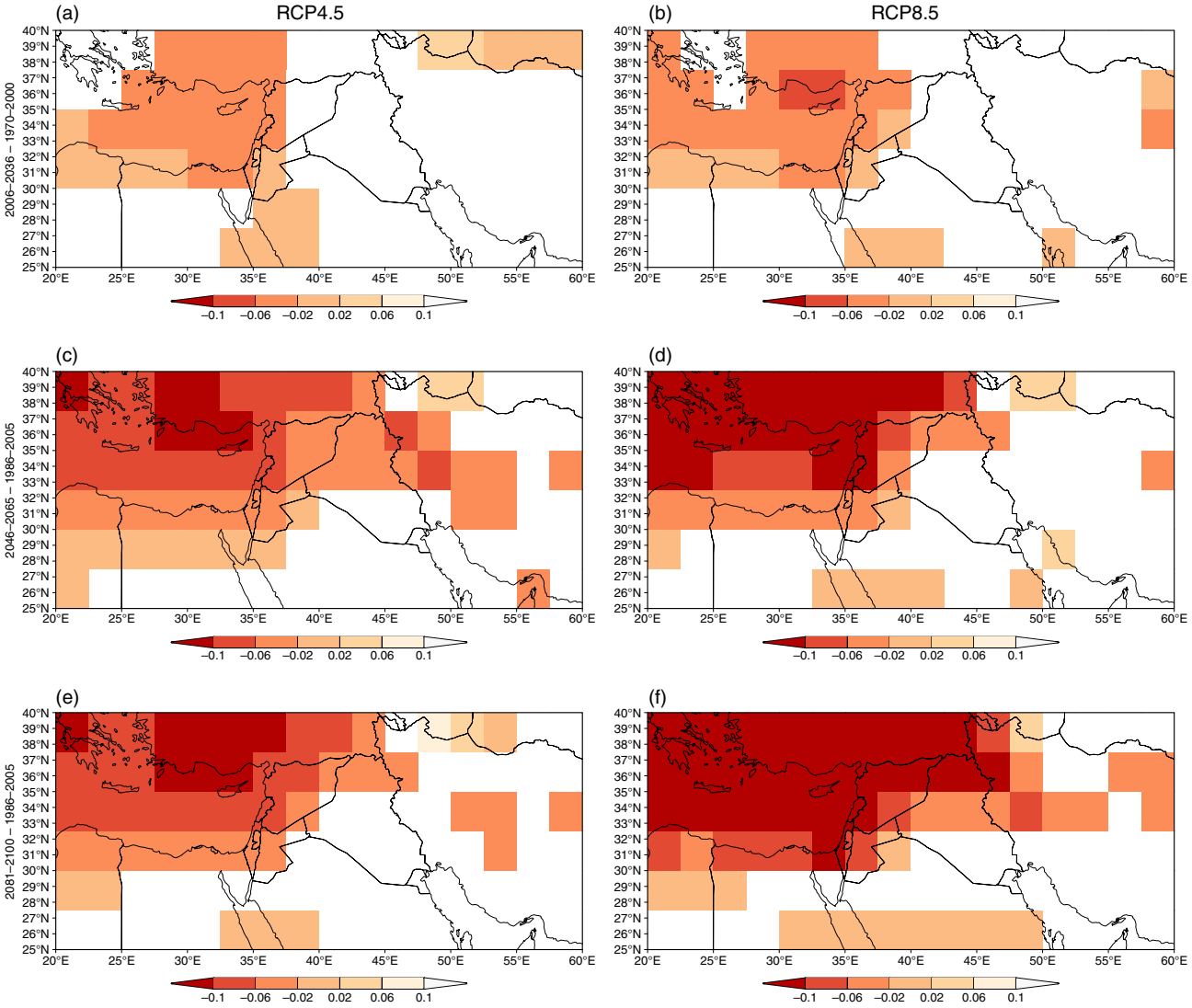

Figure 7. The CMIP5 ensemble mean of 'future minus present' for daily rainfall intensity RCP4.5 (left column) and RCP8.5 (right column) calculated for the wet days only (mm/days). Three future periods are considered 2006–2036 (a, b), 2046–2065 (c, d), and 2081–2100 (e, f).The two historical periods are 1970–2000 and 1986–2005. [Colour figure can be viewed at wileyonlinelibrary.com].

for TP in most of the models, but not for CWD, P95, and R1mm, in which APHRODITE observations is located within the model spread (Figures 4(a), (c), (e), and (g)). Thus, the 1-mm threshold for number of wet days and number of CWD is reasonable coinciding with Hochman *et al.* (2017b), which found that about 20% of the days are classified as precipitation producing systems (Goldreich, 2003).

When considering changes in the duration of wet spells, it is important to account for the relative contribution of wet spells of a specific length to the total number of wet spell events and to the total number of wet days. Presented in Figures 5(a) and (b), respectively. This may help to eliminate the impact of inter-annual changes in the number of wet days (Zolina *et al.,* 2013). It is shown that in the small study area the probability of a long wet spell (≥6 days) is <3% of the wet spells (Figure 5(a)) and <1% of the total number of wet days (Figure 5(b)). The probability of a short wet spell of 1 day duration is ≈33% of the wet spells (Figure 5(a)) and ≈12% of the total number of wet days (Figure 5(b)).

In summary, CMIP5 models performance was evaluated for their ability to capture the spatial, temporal, and statistical properties of APHRODITE daily precipitation observations. In general, the models ensemble mean was found to perform relatively well for the purpose of analysing trends of different EPIs, especially for the indices TP, CWD, P95, and R1mm. Abramowitz and Gupta (2008) have discussed the usage of independent models in an ensemble mean approach to reduce percentage bias. Although some of the models probably share atmospheric and oceanic code, coming from the same family of models (e.g. HadGEM2, MPI, GFDL an IPSL model families), they do not present exactly the same temporal and statistical features, as shown above, and were considered as independent. Thus, assumed to contribute information to the ensemble mean used in the following sections. Furthermore, as the trend of EPI is the focus of this study this issue is not as important,

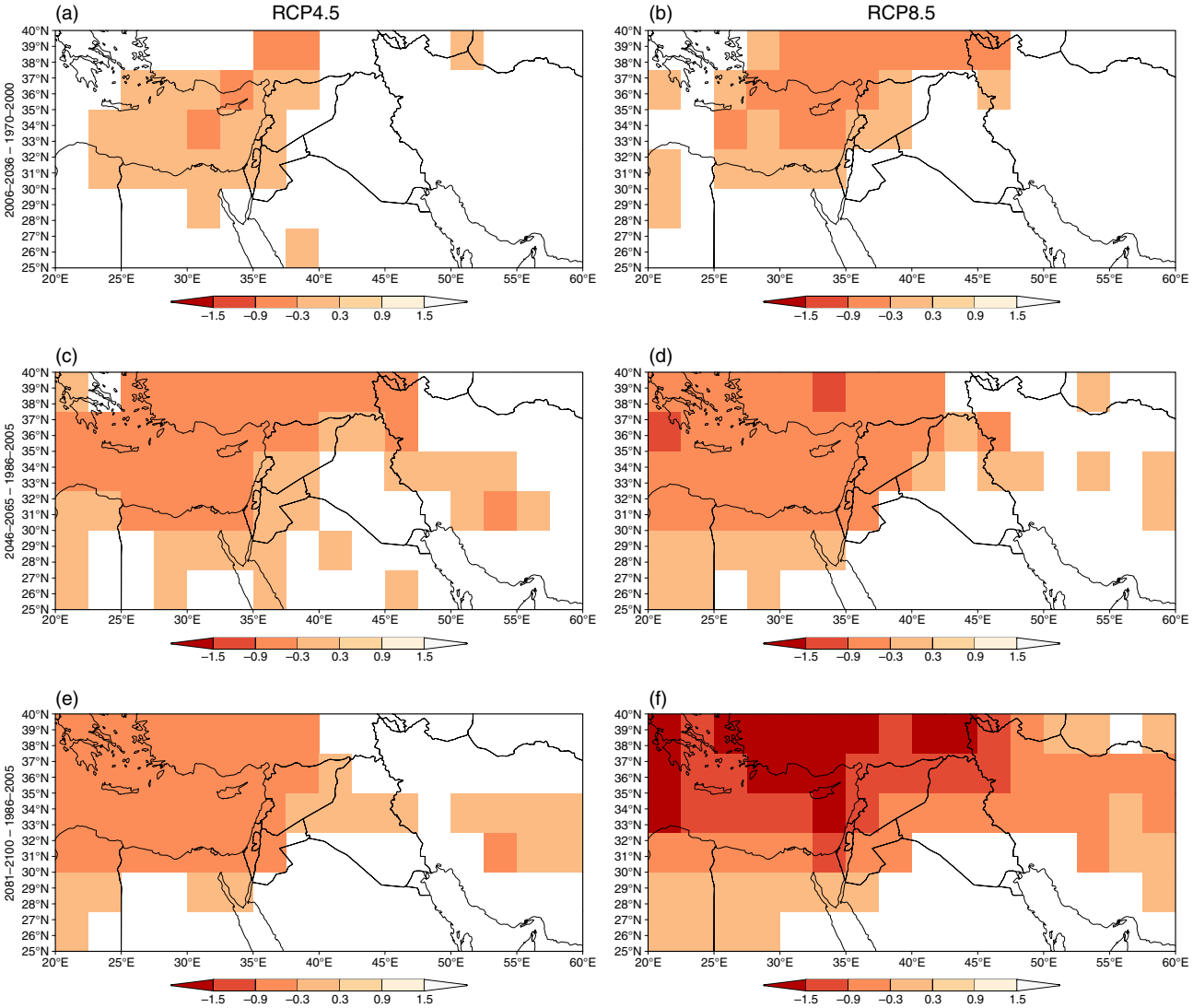

Figure 8. Same as Figure 6 but for the CWD index (in days). [Colour figure can be viewed at wileyonlinelibrary.com].

since all models' trends were also calculated separately. This experiment provides insight for future downscaling studies, which will be performed in a following study.

Note that two additional experiments were performed (not shown): (1) calculating the ensemble mean for the four chosen EPI using only the 'better' models, (2) calculating the ensemble mean using only the models that definitely do not share code and therefore are considered independent. In both cases, no significant differences were found that might change the main conclusions of this study. Thus, the ensemble mean in the following sections was calculated using all available model simulations, considered as the best estimate for the various EPI.

4.2. Present to future predictive skill

Figure 6 presents the portrait diagrams for the small (Figure 6(a)) and large (Figure 6(b)) study areas, indicating the difference in percentage between the models' 2006–2036 and 1970–2000 periods, for the RCP4.5 scenario.

As mentioned earlier, these 'decadal predictions' were initialized based on observations and reflect, on top of the projected change, both the predictability of climate change and the predictive skill of the forecast system. Figure 5, reveals an agreement among the models for future rainfall increase in the upper tenth percentile, at least for the large study area, an increase in the duration of consecutive dry days and a decrease in the duration of CWD.

The majority, i.e. 18 of 23 and 15 of 23 models, show a decrease of 10–20% in TP for both the small (Figure 6(a)) and the large (Figure 6(b)) study areas, respectively. Twenty-one of the 23 models show a decrease of up to 20% in R1mm for the small area (Figure 6(a)), while 15 of the 23 models show a similar decrease for the large area (Figure 6(b)). For the small area, only 4 of the models show increase in P95 (Figure 6(a)), whereas 11 of the models show an increase for the large area (Figure 6(b)). Only 6 of the 23 models show an increase in CWD, while 12 models show a decrease for both regions. Finally, the ensemble mean indicates that for the small area most EPI

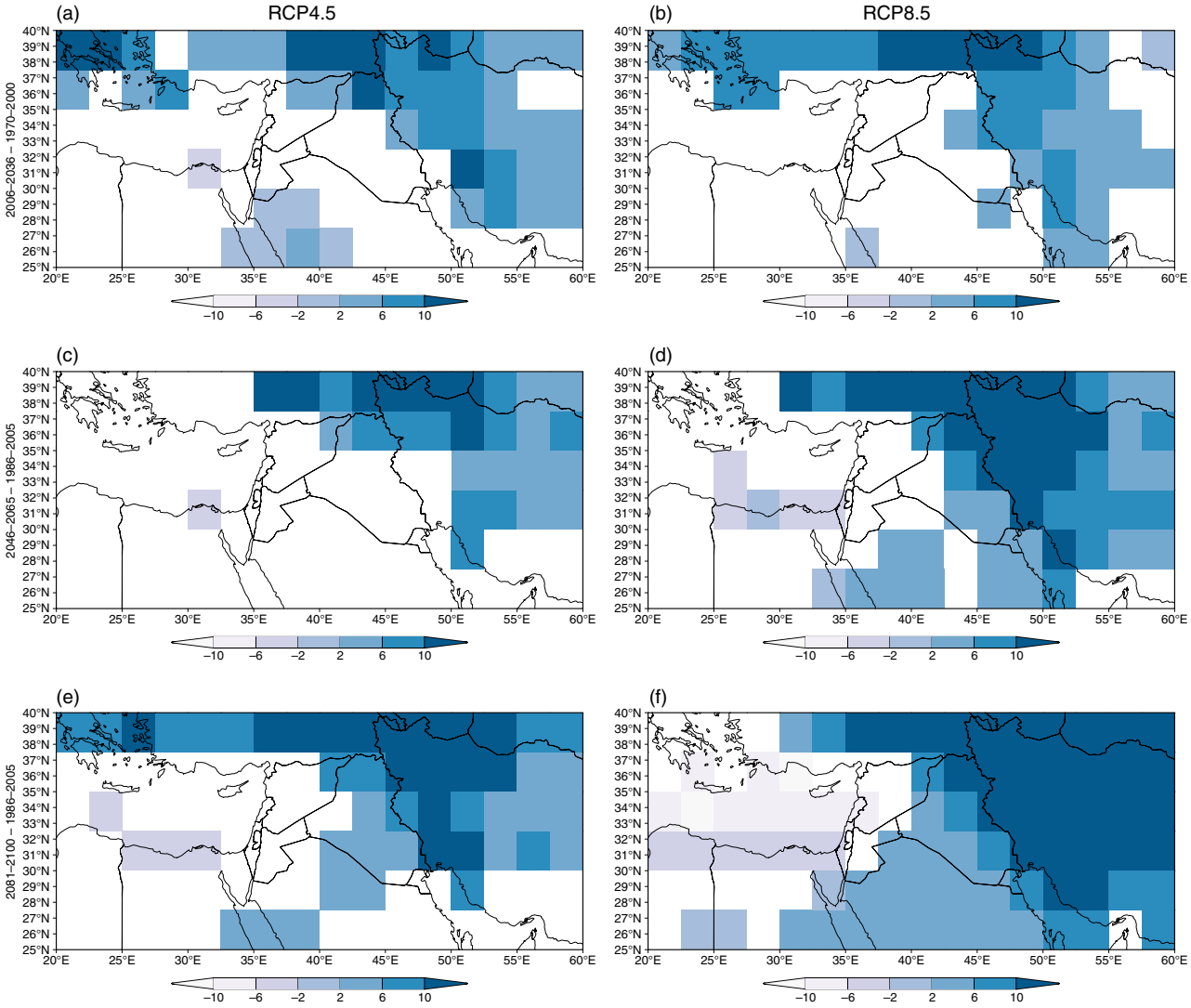

Figure 9. Same as Figure 6 but for P95 (extremely wet days) index (in mm). [Colour figure can be viewed at wileyonlinelibrary.com].

project future decreases of 10–20%, except for CDDDJF, which shows an increase of 10–20% (Figure 6(a)). For the large area increases are projected for P90, P95, CDDDJF, and CDDDJFmx (Figure 6(b)).

In summary, the CMIP5 models tend to agree that for the present–future period (2006–2036) a decrease is expected in TP with an increase in extreme precipitation at least for the large area. This will be accompanied by a decrease/increase in the length of wet/dry spells, respectively. The next section presents the spatial and temporal evolution of 4 of the 12 EPI, in more detail, and in a longer temporal perspective, including projections for the entire 21st century based on different RCP scenarios.

4.3. Spatial and temporal evolution of the EPI

Figure 7 displays difference maps between future and present simulations for the ensemble mean of TP for three future periods (2006–2036, 2046–2065, and 2081–2100) and two emission scenarios, RCP4.5 and RCP8.5. Note that TP (given in mm/days) is normalized in each grid point by the number of wet days, enabling the comparison between different regions. It is shown that a decrease in TP is projected for the small study area, especially in the Taurus Mountains (southern Turkey).

This decrease is projected to aggravate based on the RCP8.5 scenario. As time progresses, towards the end of the 21st century, the decrease is projected to cover the entire EM, including the FC, except for a small region in Northern Iran and the Caspian Sea, which shows TP increase.

Figure 8 shows the same as Figure 7 but for the CWD index. Significant decrease of CWD is projected for the small area, of about 1 day in the RCP4.5 scenario (Figure 8(e)) and about 2 days in the RCP8.5 scenario (Figure 8(f)) by the end of the 21st century.

Figure 9 shows the results for the P95 index. The extreme precipitation is projected to intensify in the FC, in spite of TP decreases as shown for the whole Mediterranean for present climate (Alpert *et al.,* 2002). However, for the small area significant decrease in the extreme precipitation is projected in both scenarios, particularly

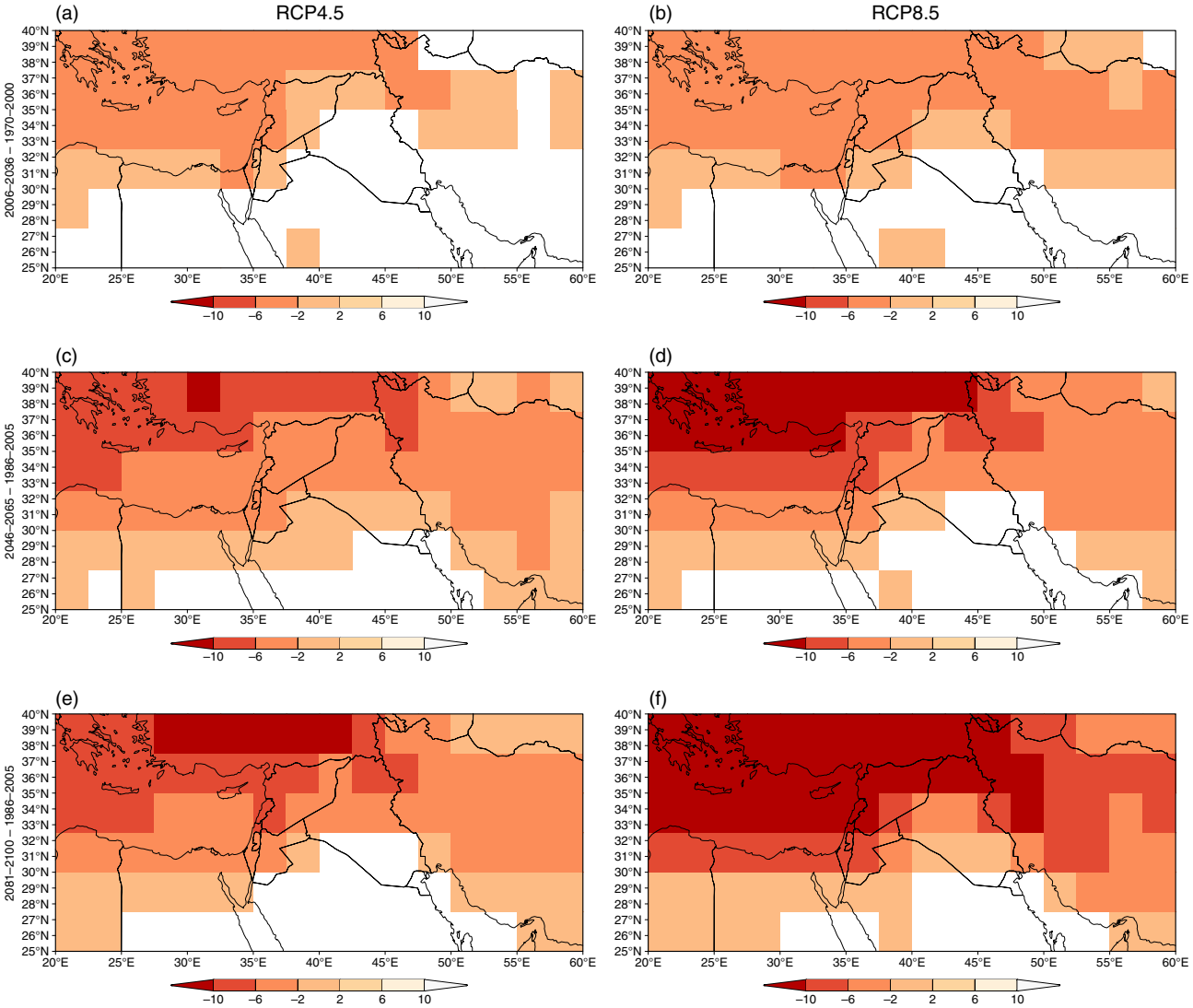

Figure 10. Same as Figure 6 but for R1mm (number of wet days) index (in days). [Colour figure can be viewed at wileyonlinelibrary.com].

pronounced in the RCP8.5 and at the end of the 21st century (Figure 8(f)).

Figure 10 shows the results for the R1mm index, indicating that the number of wet days is projected to decrease during the 21st century over the entire EM, in agreement with the decrease of TP.

When looking at the evolution of the projected changes (Figure 11), the small study area is predicted to experience a large decrease in TP from around year 2030 in the RCP8.5 scenario (Figure 11(b)). It is projected to decrease in about 100 mm during the 1861–2100 period (Figure 11(b)), i.e. a 35% drop. This decrease is accompanied by a projected decrease in CWD of about 1 and 2 days for RCP4.5 and RCP8.5, respectively (Figures 11(c) and (d)). The P95 index does not show any significant trend for the small study area (Figures 11(e) and (f)), assuming to result from the fact that it is a spatial average of a region comprising both increasing and decreasing trends in P95 (Figure 9), counter balancing one another (Figures 11(e) and (f)).

The ensemble mean for R1mm according to the RCP4.5 scenario (Figures 11(g)) projects a decrease, in the order of 10 days for the small study area (compared to about 65 days in the beginning years of 1860s). As for the RCP8.5 scenario (Figure 11(h)) the projected decrease reaches even 20 days for the small study area, which is about a third of the total number of wet days.

Figure 12 illustrates the points in time which RCP4.5 and RCP8.5 depart from one another. This is especially important in an impacts perspective. It is shown that for TP, CWD, and R1mm the scenarios depart at approximately 2020, 2050, and 2030, respectively. For P95 no clear difference between the scenarios was observed.

Possible explanations for the changes in EPI in the 21st century may include changes in the frequency and intensity of the synoptic systems responsible for rainfall in the EM and the FC. This refers mainly to potential changes in the frequency and intensity of cyclones, changes in the European and Mediterranean storm tracks governed by the phase of the North Atlantic Oscillation (Krichak *et al.*,

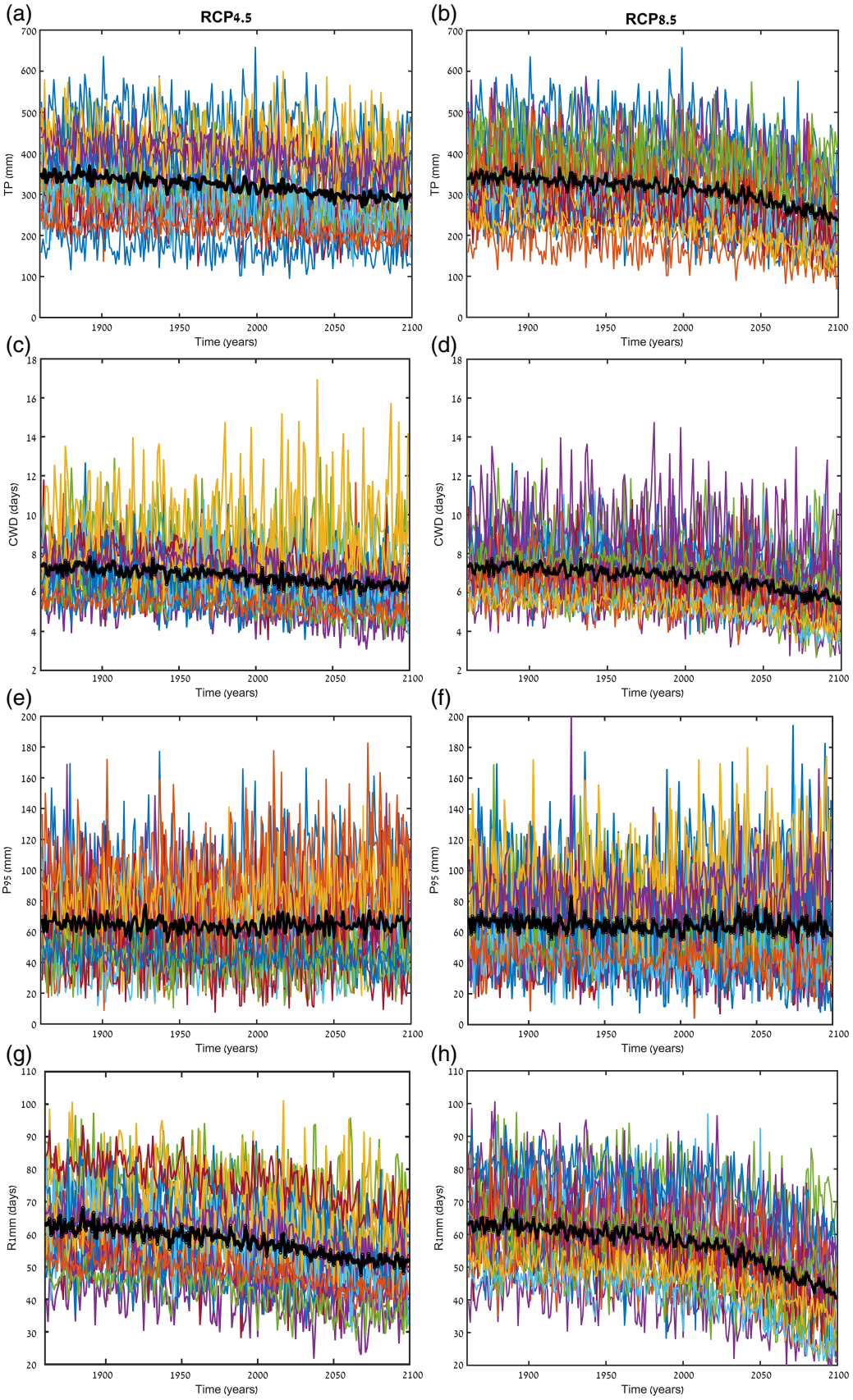

Figure 11. The evolution of TP (a, b), CWD (c, d), extremely wet days (P95; e, f) and number of wet days (R1mm; g, h)in CMIP5 models (1861–2100) for RCP4.5 (left column) and RCP8.5 (right column) over the small area. The ensemble mean of the models is marked with a bold black line. [Colour figure can be viewed at wileyonlinelibrary.com].

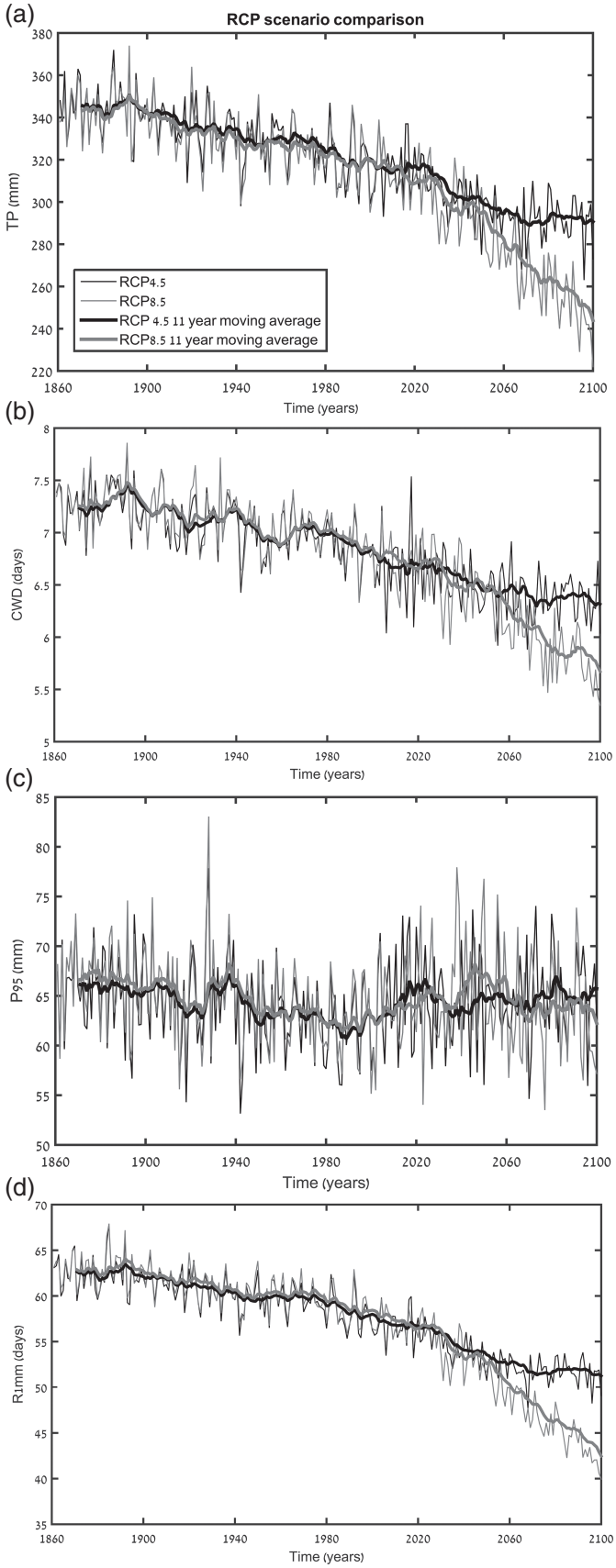

Figure 12. Same as Figure 11 showing only the RCP4.5 and RCP8.5 ensemble means for the CMIP5 models. (a) TP (mm), (b) CWD (days), (c) extremely wet days (P95; mm), (d) number of wet days (R1mm; days).

2002; Krichak and Alpert, 2005; Ziv *et al.,* 2006; Yosef *et al.,* 2009; Ziv *et al.,* 2014) and the expected expansion of the Hadley Cell towards the poles under a warmer climate (Lu *et al.,* 2007). This point was further studied in Hochman *et al.* (2017b) using a synoptic classification approach applied to 21st century CMIP5 projections.

5. Summary and conclusions

The CMIP5 project provides future projections based on several climate models. The different models are not expected to perform similarly in all parts of the globe due to their different structure and physical features. Here, the ability of 23 CMIP5 models to predict EPI is evaluated, and used to assess future projected changes in the precipitation regime over the Middle East.

There is no one model that performs the best for all EPI, and the variety of models' performance leads to large uncertainties, which the ensemble approach may significantly reduce. The ensemble mean of the 23 CMIP5 models used in this study was found to well replicate the unique shape of the precipitation gradients characterizing the FC and the EM. A general overestimations in the EPI is observed in CMIP5 models as compared to the APHRODITE data set. These overestimations are probably related to the exaggerated moisture availability in the cumulus parameterization and the inadequate representation of topography in the GCMs, due to relatively coarse spatial resolutions (Hochman *et al.,* 2017a). Regional-scale evaluations can be further developed using dynamical and statistical downscaling. The evaluation of the GCMs presented in this study may serve as a basis for exploring the potential GCMs to be used in downscaling studies for the EM and FC regions. It seems that the models perform better for the large area, however, this result is due to two main reasons: (1) as the area analysed is larger it smooths out the differences between both the models and observations, (2) specifically, in this region, incorporation of large areas which are poorly monitored (e.g. desert) in the evaluation, results in that CMIP5 models are actually compared with APHRODITE model interpolation and not with observations. The ensemble mean was proven to be useful in simulating EPI (bias $<' \pm 20\%$), except for P10, P50, CWDmx, and CWDDJFmx. For these indices the biases reached even 100% or higher, particularly for weak rains, i.e. P10. These order of overestimations in P10 can be explained by the Virga phenomenon. Since rain gages incorporated in the APHRODITE data set do not measure the precipitation produced underneath the cloud, but evaporates before it reaches the ground, and CMIP5 models do not simulate Virga accurately, due to coarse resolution, therefore producing rain even though it does not reach the ground.

The CMIP5 models tend to agree that the EM is expected to experience a decrease in TP, CWD, and R1mm of about 20–35%, 10–20%, and 20–35%, respectively, by the end of the 21st century. It is shown that P95 is projected to increase over the FC region, by about 25%, however, for the southeastern part of the Mediterranean Sea a decrease is projected, particularly for RCP8.5 scenario and towards the end of the 21st century.

It can be concluded that while TP is projected to decrease, extreme precipitation is projected to increase at least for the FC. Such a trend has been shown for the Mediterranean for the second half of the 20th century (Alpert *et al.,* 2002; Zhang *et al.,* 2005; Yosef *et al.,* 2009), though insignificant for the Middle East and Israel. The projected changes might be a result of changes in the frequency and intensity of the rain producing synoptic systems over the EM and FC (Hochman *et al.,* 2017b) especially governed by the phase of the North Atlantic Oscillation (shown, e.g. in Krichak *et al.,* 2002; Krichak and Alpert, 2005; Ziv *et al.,* 2006; Yosef *et al.,* 2009; Ziv *et al.,* 2014) and the expected expansion of the Hadley Cell towards the poles in a warmer climate (Lu *et al.,* 2007). This might influence agriculture, floods potential and water and food availability in a region already suffering from political unrest related to water and food issues (Kelley *et al.,* 2015).

Acknowledgements

We would like to thank the editor and anonymous reviewers for their valuable time and useful contributions. The inputs suggested by the reviewers definitely helped improve our manuscript. We thank the Ministry of Science and Technology of Israel and Tel-Aviv University president and Mintz foundation for their support. This study was also partially supported by cooperation in the international virtual institute DESERVE (Dead Sea Research Venue), funded by the German Helmholtz Association and by the Porter School of Environmental Studies at Tel-Aviv University. Late Dr. Rana Samuels initiated this research and continued working on this study in spite of becoming severely ill. She submitted her preliminary results by 31 March 2014 when she left to her final treatments in the USA. Rana passed away on 23 October 2014. This article is dedicated to her blessed memory.

References

Abramowitz G, Gupta H. 2008. Toward a model space and model independence metric. *Geophys. Res. Lett.* **35**: L05705. https://doi.org/10.1029/2007GL032834.

Alpert P, Neeman BU, Shay-El Y. 1990. Climatological analysis of Mediterranean cyclones using ECMWF data. *Tellus* **42A**: 65–77.

Alpert P, Ben-Gai T, Baharad A, Benjamini Y, Yekutieli D, Colacino M, Diodato L, Ramis C, Homar V, Romero R, Michaelides S, Manes A. 2002. Evidence for increase of extreme daily rainfall in the Mediterranean in spite of decrease in Total values. *Geophys. Res. Lett.* **29**(1536): 31–34.

Alpert P, Price C, Krichak SO, Ziv B, Saaroni H, Osetinsky I, Barkan J, Kishcha P. 2005. Tropical tele-connections to the Mediterranean climate and weather. *Adv. Geosci.* **2**: 157–160.

Alpert P, Krichak SO, Shafir H, Haim D, Osetinsky I. 2008. Climate trends to extremes employing regional modeling and statistical interpretation over the eastern Mediterranean. *Global Planet. Change* **63**: 163–170.

Chaudhary S, Dhanya CT, Vinnarasi R. 2017. Dry and wet spell variability during monsoon in gauge-based gridded daily precipitation datasets over India. *J. Hydrol.* **546**: 204–218.

Chenoweth J, Hadjinicolaou P, Bruggeman A, Lelieveld J, Levin Z, Lange MA, Xoplaki E, Hadjikakou M. 2011. Impact of climate change on the water resources of the eastern Mediterranean and Middle East region: modeled 21st century changes and implications. *Water Resour. Res.* **47**: W06506. https://doi.org/10.1029/2010WR010269.

De Vries AJ, Tyrlis E, Edry D, Krichak SO, Steil B, Lelieveld J. 2013. Extreme precipitation events in the middle-east: dynamics of the Red Sea trough. *J. Geophys. Res. Atmos* **118**: 7087–7108.

Domínguez M, Romera R, Sánchez E, Fita L, Fernández J, Jiménez-Guerrero P, Montávez JP, Cabos WD, Liguori G, Gaertner MA. 2013. Present-climate precipitation and temperature extremes over Spain from a set of high resolution RCMs. *Clim. Res.* **58**: 149–164. https://doi.org/10.3354/cr01186.

Giorgi F, Lionello P. 2008. Climate change projections for the Mediterranean region. *Global Planet. Change* **63**: 90–104.

Givati A, Rosenfeld D. 2013. The Arctic oscillation, climate change and the effects on precipitation in Israel. *Atmos. Res.* **133**: 114–124.

Goldreich Y. 2003. *The Climate of Israel: Observation, Research and Application*. Springer: Israel; Kluwer Academic/Plenum Publishers: The Netherlands, 298.

Hochman A, Bucchignani E, Gershtein G, Krichak SO, Alpert P, Levi Y, Yosef Y, Carmona Y, Breitgand J, Mercogliano P. 2017a. Evaluation of regional COSMO-CLM climate simulations over the eastern Mediterranean for the period 1979–2011. *Int. J. Climatol.* https://doi.org/10.1002/joc.5232.

Hochman A, Harpaz T, Saaroni H, Alpert P. 2017b. Synoptic classification in 21st century CMIP5 predictions over the eastern Mediterranean with focus on cyclones. *Int. J. Climatol.* https://doi.org/10.1002/joc.5260.

Huffman GJ, Adler RF, Morrissey MM, Bolvin DT, Curtis S, Joyce R, McGavock B, Susskind J. 2001. Global precipitation at one-degree daily resolution from multi-satellite observations. *J. Hydrometeorol.* **2**(1): 36–50.

IPCC. 2013. In *Climate Change 2013: The Physical Science Basis. Contribution of Working Group I to the Fifth Assessment Report of the Intergovernmental Panel on Climate Change*, Stocker TF, Qin D, Plattner GK, Tignor M, Allen SK, Boschung J, Nauels A, Xia Y, Bex V, Midgley PM (eds). Cambridge University Press: Cambridge, UK and New York, NY, 1535. https://doi.org/10.1017/CBO9781107415324.

Kelley CP, Mohtadi S, Cane MA, Seager R, Kushnir Y. 2015. Climate change in the fertile crescent and implications of the recent Syrian drought. *Proc. Natl. Acad. Sci. USA* **112**: 3241–3246. https://doi.org/10.1073/pnas.1421533112.

Kitoh A, Yatagai A, Alpert P. 2008. First super high resolution model projection that the ancient "fertile crescent" will disappear in this century. *Hydrol. Res. Lett.* **2**: 1–4.

Klein Tank AMG, Zwiers FW, Zhang X. 2009. Guidelines on analysis of extremes in a changing climate in support of informed decisions for adaptation. *Climate Data and Monitoring*, WCDMP-No. 72, WMO-TD No.1500.

Krichak SO, Alpert P. 2005. Decadal trends in the East Atlantic–West Russia pattern and Mediterranean precipitation. *Int. J. Climatol.* **25**: 183–192.

Krichak SO, Kishcha P, Alpert P. 2002. Decadal trends of main Eurasian oscillations and the Mediterranean precipitation. *Theor. Appl. Climatol.* **72**: 209–220.

Krichak SO, Alpert P, Dayan M. 2004. The role of atmospheric processes associated with Hurricane Olga in the December 2001 floods in Israel. *J. Hydrometeorol.* **5**: 1259–1270. https://doi.org/10.1175/JHM-399.1.

Krichak SO, Alpert P, Kunin P. 2010. Numerical simulation of seasonal distribution of precipitation over the eastern Mediterranean with a RCM. *Clim. Dyn.* **34**(1): 47–59.

Krichak SO, Barkan J, Breitgard JS, Gualdi S, Feldstein SB. 2015. The role of the export of tropical moisture into mid-latitudes for extreme precipitation events in the eastern Mediterranean region. *Theor. Appl. Climatol.* **121**: 499–515.

Lelieveld J, Hadjinicolaou P, Kostpoulou E, Chenoweth J, El Maayer M, Giannakopoulos C, Hannides C, Lange MA, Tanarhte M, Tyrlis E, Xoplaki E. 2012. Climate change and impacts in the eastern Mediterranean and the Middle East. *Clim. Change* **114**: 667–687.

Lu J, Vecchi GA, Reichler T. 2007. Expansion of the Hadley cell under global warming. *Geophys. Res. Lett.* **34**: L06805. https://doi.org/10.1029/2006GL028443.

Meehl GA, Covey C, Delworth T, Latif M, McAvaney B, Mitchell JFB, Stouffer RJ, Taylor KE. 2007. The WCRP CMIP3 multi-model dataset: a new era in climate change research. *Bull. Am. Meteorol. Soc.* **88**: 1383–1394.

New MG, Hulme M, Jones PD. 1999. Representing twentieth century space-time climate variability. Part I: development of a 1961–90 mean monthly terrestrial climatology. *J. Clim.* **12**: 829–856.

Raich R, Alpert P, Messer H. 2017. Vertical precipitation estimation using microwave links in conjunction with weather radar. In *15th International Conference on Environmental Science and Technology, 31st August to 2nd September 2017*, Rhodes, Greece.

Saaroni H, Halfon H, Ziv B, Alpert P, Kutiel H. 2010. Links between the rainfall regime in Israel and location and intensity of Cyprus lows. *Int. J. Climatol.* **30**: 1014–1025.

Samuels R, Smiatek G, Krichak S, Kunstmann H, Alpert P. 2011. Extreme value indicators in highly resolved climate change simulations for the Jordan River area. *J. Geophys. Res.* **116**: D24123. https://doi.org/10.1029/2011JD016322.

Shalev S, Saaroni H, Izsak T, Yair Y, Ziv B. 2011. The spatio-temporal distribution of lightning over Israel and the neighboring area and its relation to regional synoptic systems. *Nat. Hazard Earth Syst. Sci.* **11**: 2125–2135.

Sillman J, Roeckner E. 2008. Indices for extreme events in projections of anthropogenic climate change. *Clim. Change* **86**: 83–104.

Sillman J, Kharin VV, Zhang X, Zwiers FW, Bronaugh D. 2013a. Climate extreme indices in the CMIP5 multi-model ensemble: part 1. Model evaluation in the present climate. *J. Geophys. Res.* **118**: 1716–1733.

Sillman J, Kharin VV, Zwiers FW, Zhang X, Bronaugh D. 2013b. Climate extreme indices in the CMIP5 multi-model ensemble: part 2. Future climate projections. *J. Geophys. Res.* **118**: 2473–2493.

Smiatek G, Kunstmann H, Heckl A. 2011. High resolution climate change simulations for the Jordan River area. *J. Geophys. Res.* **116**: D16111. https://doi.org/10.1029/2010JD015313.

Soares PMM, Cardoso RM, Miranda PMA, Viterbo P, Belo-Pereira M. 2012. Assessment of the ENSEMBLES regional climate models in the representation of precipitation variability and extremes over Portugal. *J. Geophys. Res.* **117**: D07114. https://doi.org/10.1029/2011JD016768.

Taylor KER. 2001. Summarizing multiple aspects of model performance in a single diagram. *J. Geophys. Res.* **106**(D7): 7183–7192.

Taylor KER, Stouffer J, Meehl GA. 2012. An overview of CMIP5 and the experiment design. *Bull. Am. Meteorol. Soc.* **93**: 485–498.

Tebaldi C, Hayhoe K, Arblaster JM, Meehl GA. 2006. Going to the extremes an inter-comparison of model-simulated historical and future changes in extreme events. *Clim. Change* **79**: 185–211. https://doi.org/10.1007/s10584-006-9051-4.

Turco M, Zollo AL, Ronchi C, De Luigi C, Mercogliano P. 2013. Assessing gridded observations for daily precipitation extremes in the Alps with a focus on northwest Italy. *Nat. Hazard Earth Syst. Sci.* **13**: 1457–1468. https://doi.org/10.5194/nhess-13-1457-2013.

Yatagai A, Alpert P, Xie P. 2008. Development of a daily gridded precipitation data set for the Middle East. *Adv. Geosci.* **12**: 1–6.

Yatagai A, Kamiguchi K, Arakawa O, Hamada A, Yasutomi N, Kitoh A. 2012. APHRODITE: constructing a long-term daily gridded precipitation dataset for Asia based on a dense network of rain gauges. *Bull. Am. Meteorol. Soc.* **93**: 1401–1415.

Yin H, Donat MG, Alexander LV, Sun Y. 2015. Multi-dataset comparison of gridded observed temperature and precipitation extremes over China. *Int. J. Climatol.* **35**(10): 2809–2827.

Yosef Y, Saaroni H, Alpert P. 2009. Trends in daily rainfall intensity over Israel 1950/1-2003/4. *Open Atmos. Sci. J.* **3**: 196–203.

Zhang X, Aguilar E, Sensoy S, Melkonyan H, Tagiyeva U, Ahmed N, Kutaladze N, Rahimzadeh F, Taghipour A, Hantosh TH, Albert P, Semawi M, Karam Ali M, Said al-Shabibi MH, al-Oulan Z, Zatari T, al Dean Khelet I, Hamoud S, Sagir R, Demircan M, Eken M, Adiguzel M, Alexander L, Peterson TC, Wallis T. 2005. Trends in Middle East climate extreme indices from 1950-2003. *J. Geophys. Res.* **110**: D22104. https://doi.org/10.1029/2005JD006181.

Zhang X, Alexander L, Hegerl C, Jones P, Tank AK, Peterson TC, Trewin B, Zwiers FW. 2011. Indices for monitoring changes in extremes based on daily temperature and precipitation data. *WIREs Clim. Change* **2**: 851–870.

Ziv B, Dayan U, Kushnir Y, Roth C, Enzel Y. 2006. Regional and global atmospheric patterns governing rainfall in the southern Levant. *Int. J. Climatol.* **26**: 55–73.

Ziv B, Saaroni H, Pargament R, Harpaz T, Alpert P. 2014. Trends in the rainfall regime over Israel, 1975-2010, and their relationship to large-scale variability. *Reg. Environ. Change* **14**: 1751–1764.

Ziv B, Harpaz T, Saaroni H, Blender R. 2015. A new methodology for identifying daughter cyclogenesis: application for the Mediterranean Basin. *Int. J. Climatol.* **35**: 3847–3861.

Zolina O, Simmer C, Belyaev K, Gulev SK, Koltermann P. 2013. Changes in the duration of European wet and dry spells during the last 60 years. *J. Clim.* **26**: 2022–2047. https://doi.org/10.1175/JCLI-D-11-00498.1.

Zollo AL, Rillo V, Buchignani E, Montesarchio M, Mercogliano P. 2016. Extreme temperature and precipitation events over Italy: assessment with high-resolution simulations with COSMO-CLM and future scenarios. *Int. J. Climatol.* **36**(2): 987–1005. https://doi.org/10.1002/joc.4401.

